Research Square

Preprints are preliminary reports that have not undergone peer review.
They should not be considered conclusive, used to inform clinical practice,
or referenced by the media as validated information.

Spatiotemporal variability of air-sea CO_2 fluxes in the Northern Indian Ocean: Insights from ocean color remote sensing

Nandha Kumar M.
Central University of Karnataka
Mukeem Thoufiq Ahmed
Andhra University
Nazeera Begum Pathan
Acharya Nagarjuna University (ANU)
P. Brahmaji Rao
Acharya Nagarjuna University (ANU)
Ibrahim Shaik
ibrahimshaik.1985@gmail.com
National Remote Sensing Centre (NRSC)
Mahesh Pathakoti
National Remote Sensing Centre (NRSC)

Research Article

Keywords: Air-sea CO2 flux, NIO region, surface ocean pCO2, atmospheric pCO2

Posted Date: November 27th, 2025

DOI: https://doi.org/10.21203/rs.3.rs-8054322/v1

License: This work is licensed under a Creative Commons Attribution 4.0 International License.
Read Full License

Additional Declarations: No competing interests reported.

Spatiotemporal variability of air-sea CO_2 fluxes in the Northern Indian Ocean: Insights from ocean color remote sensing

Nandha Kumar M.[1], Mukeem Thoufiq Ahmed[2], Nazeera Begum Pathan[3], P. Brahmaji Rao[3], Ibrahim Shaik[4*] Mahesh Pathakoti[4]

[1]Central University of Karnataka, Gulbarga, India.
[2]Department of Geoengineering, Andhra University, Visakhapatnam, India.
[3]Department of Environmental Sciences, Acharya Nagarjuna University (ANU), Guntur, India.
[4]National Remote Sensing Centre (NRSC), Hyderabad, India.
*Corresponding author: ibrahimshaik.1985@gmail.com

Abstract

Quantifying sea surface pCO_2 (pCO_{2sw}), atmospheric pCO_2 (pCO_{2air}), and the CO_2 flux between these two media is essential for understanding the global carbon cycle and its interactions with climate change. Satellite based quantification offers a significant advantage in monitoring oceanic CO_2 absorption by providing continuous, widespread, and high-resolution data, thereby overcoming the limitations posed by sparse in-situ measurements particularly in the North Indian Ocean (NIO). This study integrates satellite derived datasets, regression equations, and models to estimate pCO_2 fields and compute air-sea CO_2 fluxes across the NIO region, including the Andaman Sea, Arabian Sea (AS), Lakshadweep Sea, and Bay of Bengal (BoB). Key input variables include sea surface temperature (SST), sea surface salinity (SSS), chlorophyll-a (Chla), wind speed (WS), atmospheric CO_2 concentration, and sea level pressure (SLP). A multi-parameter regression approach was used to estimate pCO_{2sw} using SST, SSS, and Chla, while pCO_{2air} was derived using atmospheric CO_2 and sea level pressure. CO_2 flux was then calculated based on ΔpCO_2, solubility coefficients, seawater density, WS, and gas transfer velocity. The results reveal a spatially diverse pattern across the NIO. The AS and Persian Gulf act as CO_2 sources, whereas the BoB and Andaman Sea serve as sinks. The Lakshadweep Sea exhibits dual characteristics, functioning both as a source and a sink depending on temporal and spatial factors. SST and Chla play significant roles in regulating sea surface pCO_2, while SSS has a minor but notable influence on the direction and magnitude of flux. These insights contribute to improving the accuracy of air-sea CO_2 flux estimation, understanding regional carbon dynamics, and projecting future trends. They also provide valuable input for shaping effective climate policies and mitigation strategies.

Key words: Air-sea CO_2 flux, NIO region, surface ocean pCO_2, atmospheric pCO_2

1. Introduction

Carbon dioxide (CO_2) is a key greenhouse gas whose atmospheric concentration has risen sharply due to anthropogenic activities, increasing at a rate of ~2 ppm/year between 2002-2011 (Ciais et al., 2013) and reaching over 420 ppm from a pre-industrial level of ~278 ppm (Ciais et al., 2013; Le Quere et al., 2018). In the ocean, CO_2 reacts with water to form carbonic acid and its dissociation products (Eq. 1-4), regulating carbon storage and contributing to ocean acidification (Doney et al., 2020).

$$H_2O + CO_2 \Leftrightarrow H_2CO_3 \quad (1)$$

$$H_2CO_3 + H_2O \Leftrightarrow HCO_3^- + H_3O^+ \quad (2)$$

$$HCO_3^- + H_2O \Leftrightarrow CO_3^{2-} + H_3O^+ \quad (3)$$

$$CO_2 + CO_3^2 + H_2O \Leftrightarrow 2\,HCO_3^- \quad (4)$$

Annually, oceans absorb ~24% of anthropogenic CO_2 emissions, making them crucial carbon sinks (Sabine et al., 2004), though this capacity is increasingly affected by the narrowing of the air-sea CO_2 partial pressure difference ($\Delta pCO_2 = pCO_{2sw} - pCO_{2air}$), which governs flux direction and intensity (Takahashi et al., 2009). Atmospheric pCO_2 has increased from ~390 µatm in 2011 to ~420 µatm (Le Quere et al., 2018; Sutton et al., 2019), reducing ocean uptake efficiency (Gruber et al., 2019). Seawater pCO_2 is influenced by sea surface temperature (SST), sea surface salinity (SSS), chlorophyll-a concentration (Chla), upwelling, biological activity, dissolved inorganic carbon (DIC), alkalinity, freshwater input, and wind speed (WS). Seasonal and regional variability in the Indian Ocean has been reported, with pCO_{2sw} reaching ~450 µatm in the Arabian Sea (AS) during monsoon driven upwelling and 320-420 µatm in the Bay of Bengal (BoB) due to freshwater input and cyclonic activity (Mangesh et al., 2021). The dual role of oceans as CO_2 sink/source is dynamic and region-specific (Joshi et al., 2020). Phytoplankton reduces pCO_{2sw} via the biological pump (Boyd et al., 2019), whereas respiration in oxygen minimum zones (OMZs) can elevate it (Rixen et al., 2020). Globally, forests absorb ~29%, oceans ~23%, and the remaining 48% of CO_2 remains in the atmosphere (Sabine et al., 2004; Khatiwala et al., 2013; Friedlingstein et al., 2024), with anthropogenic emissions contributing 90% and biological sources 10%. The Indian Ocean, one of the fastest warming basins, exhibits reduced CO_2 solubility and enhanced stratification, lowering its uptake capacity (Resplandy et al., 2023), with regional fluxes varying from a sink of 0.4-0.6 Gt C/yr to a source of -0.05 Gt C/yr, especially in the AS during monsoons, while the BoB maintains uptake that is episodically

disrupted by cyclones (Lenton et al., 2013; Sarma et al., 2013; Mangesh et al., 2021). Despite their importance, air-sea CO_2 flux estimates carry ~20-30% uncertainty due to sparse pCO_{2sw} observations and variability in gas transfer velocity (k) (Rodenbeck et al., 2014). Recent advancements in remote sensing have enabled regional scale investigation of decadal air-sea CO_2 flux variability in the Northern Indian Ocean (NIO), overcoming limitations of previous studies by integrating satellite derived parameters (SST, SSS, and Chla) with machine learning and multi-parametric regression models to capture spatial and temporal dynamics more comprehensively (Wanninkhof et al., 2013). This approach supports the development of regionally tuned models and enhances the understanding of flux variability driven by climate phenomena such as ENSO (Feely et al., 2017) and episodic events like cyclones, ultimately providing improved insights into the ocean role in the global carbon cycle. In the present study, we investigated the decadal variability of air-sea CO_2 fluxes in the NIO using a remote sensing based approach, addressing limitations of sparse in-situ observations and high uncertainties in previous estimates. We utilized satellite-derived oceanographic parameters such as SST, SSS, Chla, WS and Sea level pressure (SLP) from multi-sensor datasets to estimate sea surface pCO_{2sw}. These were then used in conjunction with atmospheric pCO_{2air} to compute ΔpCO_2 and subsequently the air-sea CO_2 fluxes using established gas exchange formulations. By utilizing high resolution, long-term remote sensing data, the present study quantifies seasonal and interannual variations and detects shifts in CO_2 sink/source behavior. This approach substantially reduces reliance on in-situ datasets, enhances spatial coverage, and provides more consistent and continuous estimates of air-sea CO_2 fluxes in the NIO, thus offering valuable insights into the oceans role in regulating atmospheric CO_2 under changing climate conditions.

1. Study region

The NIO, a semi-enclosed basin of the Indian Ocean (IO) located between 30°N-3°S and 14.5°E-103.5°E, is surrounded by the Asian landmass to the north and exhibits unique oceanographic and biogeochemical characteristics compared to the other major ocean basins (Schott and McCreary, 2001) (Fig. 1). In this study, the NIO was divided into distinct sub regions based on the MarineRegions.org classification (Flanders Marine Institute, 2019) to capture the spatial variability in CO_2 flux dynamics more effectively. The analysis focused primarily on the AS (25.6°N-1°S; 51°E-74.1°E), BoB (23°N-5.9°N; 78.9°E-95°E), Andaman Sea (17.3°N-5.6°N; 92.3°E-98.9°E), and Lakshadweep Sea (14.8°N-0.7°S; 71.9°E-80.6°E), each exhibiting distinct

physical and biogeochemical regimes (Bates et al., 2006; Kumar et al., 2004). The BoB and Andaman Sea are characterized by significant freshwater influx and strong stratification due to major river discharges (Prasanna Kumar et al., 2012), while the AS is dominated by seasonal upwelling and high biological productivity driven by monsoonal forcing (Madhupratap et al., 1996). The Lakshadweep Sea, by contrast, represents more oligotrophic open ocean conditions with minimal terrestrial influence (Antony et al., 2021).

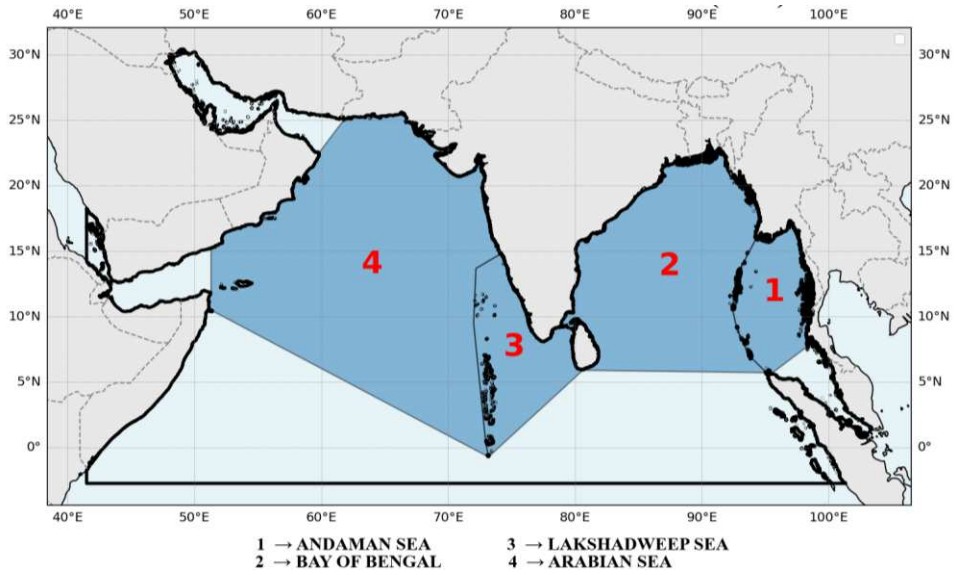


Fig.1 depicts the NIO study region

Additional regions, including the Persian Gulf, Gulf of Oman, Strait of Hormuz, Bab el-Mandeb, Gulf of Aden, and adjacent equatorial waters, were also included to provide a comprehensive understanding of the broader NIO CO_2 flux patterns. This regional categorization allows for better interpretation of the spatial heterogeneity in air-sea CO_2 exchange driven by varying physical forcings, freshwater inputs, and biological activity (Sabine et al., 2004; Takahashi et al., 2009).

2. Satellite data

As this study focuses on the estimation of air-sea CO_2 flux, we utilize long-term, monthly remote sensing datasets from various sources for key oceanographic and atmospheric variables. SST and Chla were obtained from MODIS-Aqua with ~9 km spatial resolution, while SSS and WS data were acquired from the Copernicus Marine Environment Monitoring Service (CMEMS). In addition, SLP and atmospheric CO_2 were sourced from the Copernicus Atmosphere Monitoring Service (CAMS) (Table1). SST, a crucial physical parameter, influences the solubility of CO_2 in seawater, with lower temperatures enhancing CO_2 solubility, thereby reducing surface pCO_2

levels. SST is governed primarily by solar radiation and varies both spatially and temporally due to diurnal heating, latitude, and oceanographic processes like upwelling. SSS reflects the salt concentration in surface waters and is influenced by freshwater input from rivers, precipitation, evaporation, and ice melt. SSS affects pCO_2 indirectly by modifying ionic strength, which alters carbonate chemistry and the solubility of CO_2. Chla, representing phytoplankton biomass, plays a crucial biological role by removing CO_2 from surface waters via photosynthesis and contributing to vertical carbon export through the biological pump. Chla variability is often associated with nutrient availability, river discharge, and upwelling. WS regulates gas exchange rates across the ocean-atmosphere interface, with stronger winds enhancing CO_2 flux through increased turbulence and boundary layer mixing. Moreover, wind driven upwelling can bring CO_2 rich deep waters to the surface, influencing surface pCO_2 concentrations. SLP represents the atmospheric pressure at sea level and governs wind patterns and weather systems, including cyclonic and anticyclonic activity, which indirectly affects CO_2 flux dynamics. Atmospheric CO_2 concentration, expressed in parts per million (ppm), is a critical driver of the air-sea CO_2 gradient. It varies spatially and temporally due to anthropogenic emissions, biomass burning, and natural processes, and is a key input in calculating atmospheric pCO_2. Higher atmospheric CO_2 concentrations can suppress CO_2 efflux from the ocean to the atmosphere and contribute to long-term ocean acidification, further influencing carbon cycle dynamics in the marine system.

Parameters	**Sensor/ Model**	**Resolution**	**Resampled**	**Source**
SST	MODIS-Aqua	0.09º	0.75º	https://oceancolor.gsfc.nasa.gov/l3/
Chla	MODIS-Aqua	0.09º	0.75º	https://oceancolor.gsfc.nasa.gov/l3/
SSS	CMEMS	0.083º	0.75º	https://doi.org/10.48670/moi-00021
Wind speed	CMEMS	0.083º	0.75º	https://doi.org/10.48670/moi-00181
Sea Level Pressure	CAMS EGG4	0.75º	0.75º	https://ads.atmosphere.copernicus.eu/datasets/cams-global-ghg-reanalysis-egg4
Atmospheric CO_2	CAMS EGG4	0.75º	0.75º	https://ads.atmosphere.copernicus.eu/datasets/cams-global-ghg-reanalysis-egg4

Table 1 Details of the datasets used for the study.

2.1. Data processing

The primary variables used in this study include monthly mean SST, SSS, Chla, WS, Atmospheric CO_2, and SLP. These datasets were acquired in Network Common Data Format (NetCDF) from various reliable sources (Table 1). To ensure spatial consistency across all variables, each dataset was resampled to a uniform spatial resolution of 0.75° × 0.75° using the nearest neighbor resampling technique, which preserves original pixel values without introducing averaging or smoothing artifacts. Prior to resampling, quality flags and invalid data points (land, clouds, and missing values) were masked using standard variable specific thresholds and flags provided by the data producers. After spatial harmonization, all datasets were temporally collocated by aligning their time coordinates to a common monthly temporal resolution. This step ensured that each grid cell across variables corresponds to the same temporal instance, thereby facilitating accurate pixel-wise comparisons and computations during the estimation air-sea CO_2 fluxes.

3. Methods of the study

3.1. Computation of air-sea CO_2 flux

The air-sea CO_2 flux represents the transfer of CO_2 across the ocean atmosphere interface and plays a crucial role in understanding the global carbon cycle and climate regulation. This flux is determined by several parameters, including the gas transfer velocity (k), the CO_2 solubility constant ($K_H^{CO_2}$), wind speed dependent coefficient (C_2), seawater density (ρ), and the difference in CO_2 partial pressure between the ocean and atmosphere (ΔpCO_2). The calculation follows the formulation outlined in Eq. 5, based on the work of Wanninkhof (1992; 2014). The detailed methodology adopted for the study was represented in Fig. 2.

$$\text{Flux} = \Delta pCO_2 * K_H^{CO2} * \rho * C_2 * k * 24 * 0.01 \qquad (5)$$

Where

$$\Delta pCO_2 = (pCO_{2sw} - pCO_{2air}) \qquad (6)$$

pCO_{2sw} = Partial pressure of CO_2 in seawater (µatm)

pCO_{2air} = Partial pressure of CO_2 in atmosphere (µatm)

K_H^{CO2} = Dissolution coefficient of CO_2 (mol/kg/atm)

ρ = Sea water density (in kg/m^3)

C_2 = Wind speed coefficient

k =Gas transfer velocity (in cm/hr)

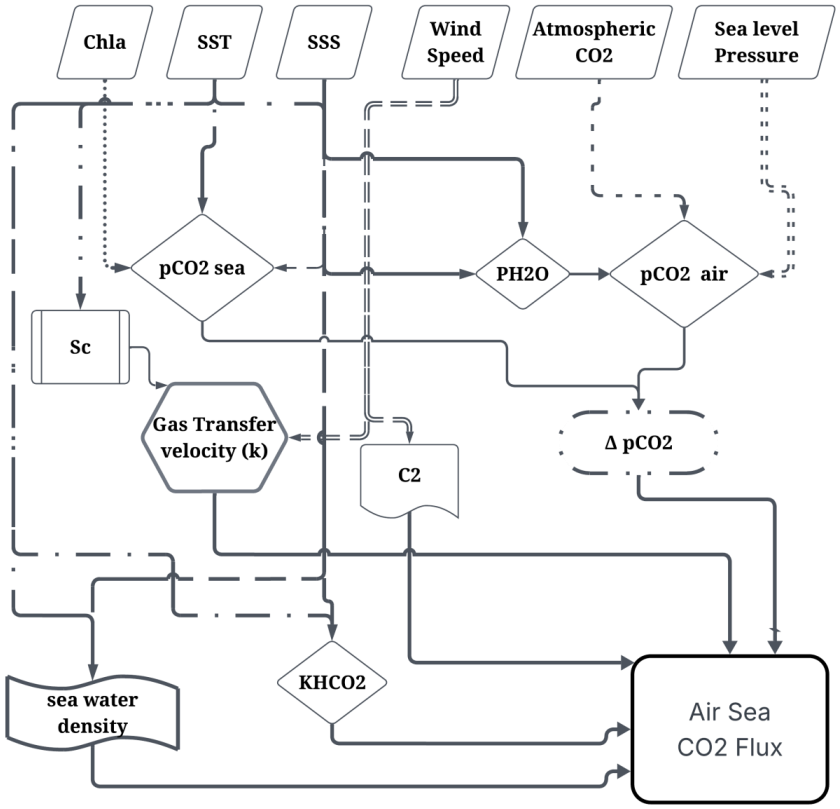


Fig. 2 represents the methodology adopted for the study.

3.2. Computing dissolution coefficient ($K_H^{CO_2}$)

The dissolution coefficient of CO_2 is crucial for estimating the air-sea CO_2 flux, as it represents the efficiency of CO_2 diffusion at the ocean atmosphere interface. This coefficient is also referred to as Henry's Law constant for carbon dioxide in seawater. The equation proposed by Sunquist (1985) was used for the analysis, incorporating SST and SSS, which are key influencing factors, along with turbulence, upwelling, and other oceanographic processes (Sunquist 1985). Accurately modeling K_HCO_2 is essential for improving observations and understanding of the carbon cycle within the Earth system.

$$lnK_H^{CO2} = -60.2409 + 93.4517 * \left(\frac{100}{T}\right) + 23.3585 * \ln\left(\frac{T}{100}\right) + S * \left[0.023517 - 0.023656 * \left(\frac{T}{100}\right) + 0.047036 * \left(\frac{T}{100}\right)^2\right] \quad (7)$$

Where T is the temperature of sea surface in Kelvin (SST + 273.15) and S is the salinity present in the sea surface in PSU.

3.3. Computing sea water density (ρ):

Calculating the density of seawater is essential, as the mobility of gases is influenced by the density of the medium. Therefore, accurate estimation of seawater density plays a significant role in understanding the dynamics of gas exchange between the ocean and atmosphere (Millero 2013).

$$\rho = \left(\rho_w + A * S + B * S^{3/2} + C * (S)^2\right) * 10^{(-3)}) \qquad (8)$$

Where A, B, C are the constants derived from the calculations. S is the Salinity of the Sea water and ρ_w is density of the pure water. This can be calculated by using the Eq. 9.

$$\rho_w = 999.842594 + 6.793952 * 10^{(-2)} * SST - 9.09529 * 10^{(-3)} * (SST)^2 + 1.001685 * 10^{(-4)} * (SST)^3 - 1.120083 * 10^{(-6)} * (SST)^4 + 6.536332 * 10^{(-9)} * (SST)^5 \qquad (9)$$

$$A = 0.824493 - 4.0899 * 10^{(-3)} * SST + 7.6438 * 10^{(-5)} * (SST)^2 - 8.2467 * 10^{(-7)} * (SST)^3 + 5.3875 * 10^{(-9)} * (SST)^4 \qquad (10)$$

$$B = 5.72466 * 10^{(-3)} + 1.0227 * 10^{(-4)} * SST - 1.6546 * 10^{(-6)} * (SST)^2 \qquad (11)$$

$$C = 4.8314 * 10^{(-4)} \qquad (12)$$

3.4. Computing wind speed coefficient (C_2)

The wind speed coefficient (C_2) in the air-sea CO_2 flux calculation is used to account for wind speed variability when estimating monthly average fluxes, as opposed to daily fluxes. It adjusts the gas transfer velocity to reflect the non-linear relationship between WS and gas exchange. This correction is necessary to capture changes in WS over the course of a month (Wanninkhof et al., 2002).

$$C_2 = \frac{(U_j^2)mean}{(U_{mean})^2} \qquad (13)$$

Where U_j is WS (daily) and U_{mean} is WS (monthly averaged).

3.5. Computing gas transfer velocity

Gas transfer velocity is a key parameter in flux calculations, as it quantifies the rate at which CO_2 molecules are exchanged between the ocean and atmosphere, playing a crucial role in the global carbon cycle. It is influenced by air velocity near the sea surface and SST, both of which directly affect gas exchange and dissolution processes (Wanninkhof et al., 2002).

$$k_{660} = 0.39 * {U_{10}}^2 \qquad (14)$$

$$k = k_{660} * (\frac{Sc}{100})^{-0.5} \quad (15)$$

$$S_c = 2073.1 - 125.62 * SST + 3.6276 * (SST)^2 - 0.043219 * (SST)^3 \quad (16)$$

Where U_{10}^2 is the monthly average of the wind speed at 10 meters above the surface and S_c is the Schmidt number, a measure of diffusivity, which is based on SST.

4. Results and discussion

4.1. Estimation of pCO_{2sw} in the NIO region

In the present study, surface ocean pCO_2 fields over the NIO were estimated using a Multiparametric Linear Regression (MLR) approach developed by Shaik et al. (2025)**.** This method integrates both in-situ measurements and satellite-derived parameters, including SST**,** SSS**,** and Chla**,** to capture the complex biogeochemical variability influencing pCO_2 distribution. The MLR model was constructed through statistical analysis of the relationship between these variables and corresponding pCO_2 values, enabling spatially continuous estimations. The final regression equation (Eq. 16) derived from this analysis were applied to generate interannual (2011-2020) pCO_2 fields for the NIO region (Shaik et al., 2025).

pCO_{2sw} = 11.08 * SST + 4.75 * SSS - 22.76 * $\log_{10}$ (Chla) – 125.76 (16).

4.1.1. Spatiotemporal variability of interannual ocean surface pCO_2

The interannual variability of surface ocean pCO_2 in the NIO from 2011 to 2020 (Fig. 3) reveals a clear spatial and temporal heterogeneity, driven by complex biogeochemical and physical processes. Throughout the decade, pCO_2 values exhibit a general increasing trend, particularly in the AS, where values frequently exceed 400 µatm and reach up to ~460 µatm, shown by the dominant orange to red color patterns in most years (Fig. 3). In contrast, the BoB consistently demonstrates relatively lower pCO_2 levels, predominantly ranging between ~300 -370 µatm, as indicated by the prevalence of green to blue hues. This inter-basin variability is largely attributed to differences in biological productivity, freshwater influx, and oceanographic circulation. The AS, with its high evaporation rates, limited riverine input, and strong seasonal upwelling, particularly during the southwest monsoon; experiences enhanced vertical mixing and entrainment of CO_2 rich subsurface waters, contributing to elevated surface pCO_2. Additionally, intense biological productivity in this region often leads to the accumulation of respired CO_2 in deeper layers, which resurfaces during upwelling events. Conversely, the BoB receives substantial freshwater input from major rivers like the Ganges, Brahmaputra, and Irrawaddy, especially during the monsoon season, resulting in strong salinity stratification that suppresses

vertical mixing. This limits the upward transport of CO_2 rich waters and, combined with high primary production driven by nutrient inputs from river discharge and eddy activity, results in relatively lower surface pCO_2 concentrations. The year to year variations observed across the decade can be linked to both regional and basin-scale climatic phenomena such as the El Nino Southern Oscillation (ENSO) and Indian Ocean Dipole (IOD), which influence wind patterns, SST, and ocean circulation. For instance, El Nino events typically reduce monsoonal intensity and upwelling in the AS, potentially lowering surface pCO_2 temporarily, while La Nina events enhances these processes. Moreover, anomalously warm SSTs associated with positive IOD or El Nino years (2014, 2015, 2016, 2018 and 2019) reduce CO_2 solubility, thereby elevating pCO_2 levels in surface waters.

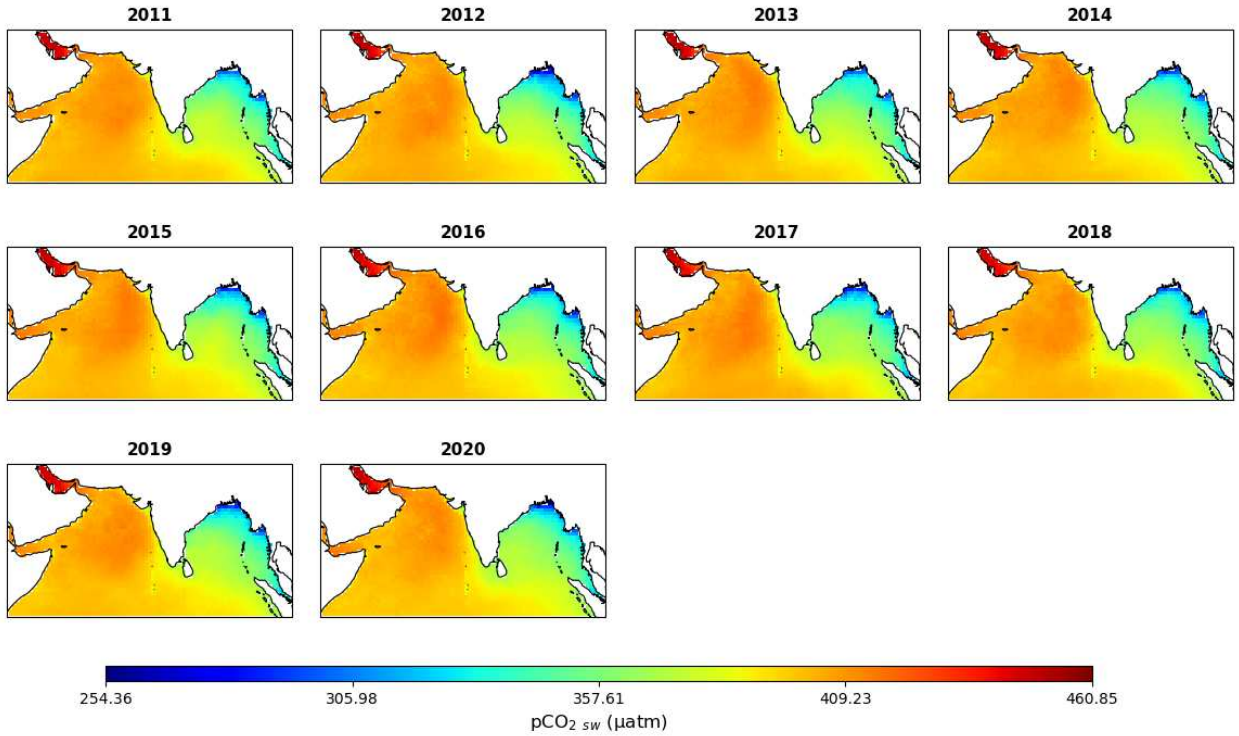


Fig. 3 Interannual variability of pCO_{2sw} in the NIO region (2011-2020).

Anthropogenic CO_2 uptake by the ocean and increasing atmospheric CO_2 concentrations further contribute to the long term rise in surface ocean pCO_2 values across the NIO. The combined effects of these natural and anthropogenic factors evident in the interannual variability observed in the decadal dataset. Furthermore, changes in regional wind speed, ocean currents, and biological activity driven by nutrient dynamics and light availability play a secondary but significant role in modulating pCO_2. It is also noteworthy that the western AS consistently shows the highest pCO_2 values due to persistent upwelling zones near the Omani and Yemeni coasts.

Overall, the observed interannual variability of surface pCO_2 in the NIO is a product of the dynamic interplay between atmospheric forcing, oceanographic processes, and biogeochemical responses, emphasizing the sensitivity of this region to both climate variability and long term environmental change.

4.1.2. Climatological variability of ocean surface pCO_2

The climatological variability of surface ocean pCO_2 in the NIO (Fig. 4) shows pronounced seasonal dynamics influenced by monsoonal circulation, biological productivity, temperature, salinity, and regional hydrodynamics. From January to March, pCO_2 levels across the AS and BoB remain relatively moderate, with the AS exhibiting slightly higher concentrations (~360-400 µatm) due to weak winter convection that enhances vertical mixing and brings CO_2 rich subsurface waters to the surface. During this period, cooler SST increase CO_2 solubility, moderating the overall pCO_2 despite vertical CO_2 fluxes. As the intermonsoonal period begins in April and May, increasing SST reduce CO_2 solubility, especially in the AS, resulting in a rise in surface pCO_2 levels (>400 µatm in some regions). The onset of the southwest (SW) monsoon in June through August marks a significant shift in pCO_2 patterns. In the AS, intense coastal upwelling driven by strong southwesterly winds along the Omani and Indian coasts leads to the resurfacing of CO_2 rich deeper waters, contributing to elevated pCO_2 levels often exceeding 430 µatm. Simultaneously, enhanced biological productivity induced by nutrient rich upwelled waters acts to draw down pCO_2 locally through photosynthetic CO_2 uptake. However, this biological drawdown is often exceeded by the physical supply of CO_2 from upwelling, resulting in net pCO_2 increases. In contrast, the BoB, under the influence of heavy monsoonal precipitation and substantial river runoff (Ganges-Brahmaputra system), exhibits reduced salinity and strong vertical stratification that suppresses mixing. This leads to comparatively lower pCO_2 values (~310-360 µatm), despite high nutrient input, due to limited entrainment of subsurface CO_2 and enhanced biological utilization of surface CO_2. The northeastern Bay in particular maintains low pCO_2 values during this period due to persistent low salinity and high productivity. In the post monsoon season (September to November), the AS begins to exhibit a decline in pCO_2 levels as upwelling subsides, biological productivity decreases, and SST begin to decrease, increasing CO_2 solubility. Meanwhile, the BoB continues to show moderate pCO_2 levels due to lingering freshwater input and stabilized stratification. December marks the onset of the northeast (NE) monsoon, characterized by dry winds from the Indian subcontinent and

cooling SST, particularly over the northern AS. This cooling increases CO_2 solubility, leading to a reduction in surface pCO_2, despite some convective mixing that brings subsurface CO_2 to the surface. Overall, the AS exhibits higher seasonal pCO_2 variability due to the strong influence of monsoonal upwelling and temperature driven solubility changes, whereas the BoB displays a more subdued seasonal cycle, dominated by stratification and freshwater fluxes. These climatological patterns emphasize the sensitivity of pCO_2 to seasonal ocean atmosphere interactions and highlight the contrasting biogeochemical regimes of the two sub basins within the NIO, which are essential for understanding regional carbon fluxes and predicting future responses to climate change.

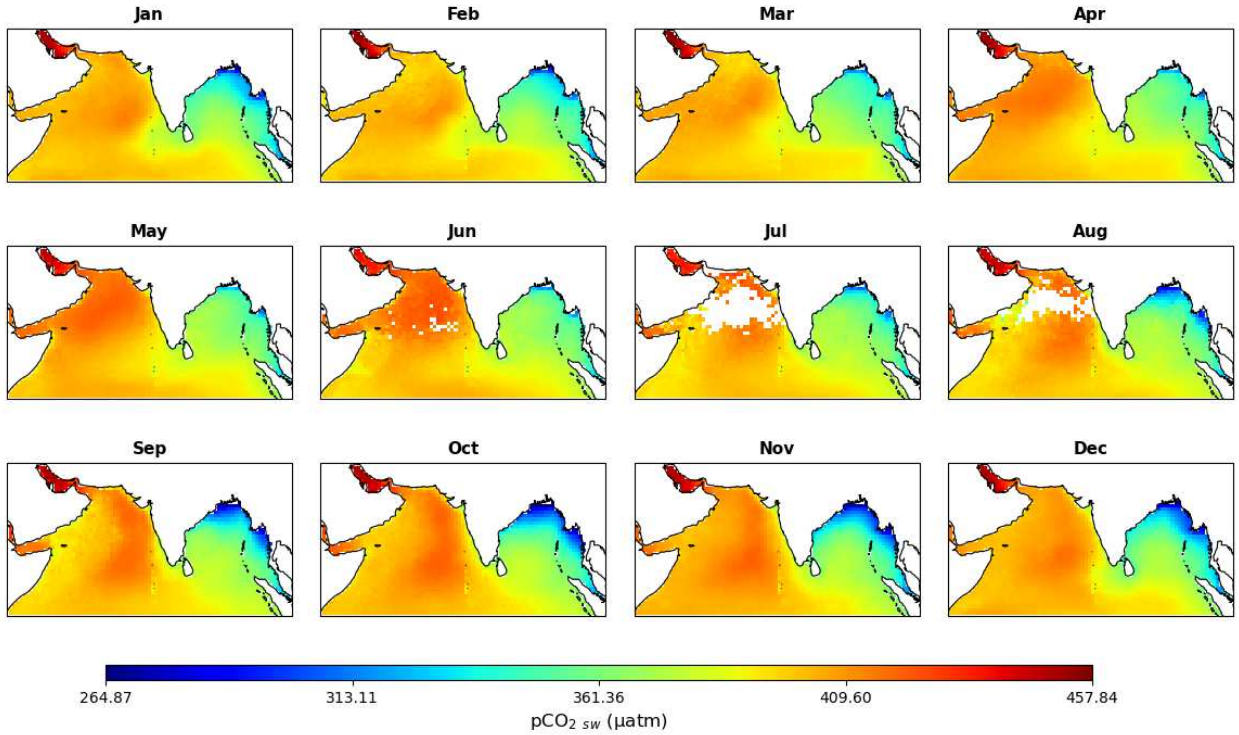


Fig. 4 Climatological variability of pCO_{2sw} in the NIO region.

4.2. **Estimation of atmospheric pCO_2**

The pCO_2 in the atmosphere (pCO_{2air}) is the measurement of pressure exerted by the concentration of the CO_2, which prevails in the atmosphere. This is the counterpart of pCO_{2sw} in the estimation of air-sea flux of CO_2. It is important for the identification of the available CO_2 present in the atmosphere for the dissolving in the ocean. This is important for the understanding the cycle of carbon within the system of the earth. pCO_{2air} was estimated using Eq. 17 (Dickson and goet, 1994, Dickson et al., 2007).

$$pCO_{2\,(air)} = XCO_2 * (P_T - P_{H2O}) \qquad (17)$$

Where XCO_2 is the mole fraction of CO_2 in the atmosphere in ppm (parts per million) and P_T is the sea level pressure in the atmosphere in the units of atm, P_{H2O} is the saturation of the vapour pressure of sea water in the atmosphere in the units of atm. The formula used in the analysis was given by (Weiss and Prince, 1980) as follows.

$$P_{H_2O} = exp\left(24.4543 - 67.4509 * \left(\frac{100}{T}\right) - 4.8489 * \ln\left(\frac{T}{100}\right) - 0.000544 * S\right) \quad (18)$$

Where T is the temperature of sea surface in Kelvin (SST + 273.15) and S is the salinity present in the sea surface in PSU.

4.2.1. Spatiotemporal variability of interannual atmospheric pCO_2

The interannual variability of pCO_{2air} in the NIO during the period 2011-2020 exhibits a pronounced increasing trend, reflecting the global atmospheric CO_2 rise driven by anthropogenic emissions. The Fig. 5 demonstrated that, pCO_{2air} values increased steadily from relatively low levels (~365-375µatm) in the early part of the decade (2011-2013) to significantly higher concentrations exceeding 400 µatm by 2020. This progressive enhancement is primarily attributed to the continuous increase in fossil fuel combustion, land use land cover changes, and industrial emissions worldwide, leading to elevated CO_2 concentrations in the atmosphere. Regionally, the NIO interannual atmospheric pCO_2 pattern is modulated by both large scale climatic phenomena and local ocean atmosphere interactions. For instance, during strong El Nino years such as 2015-2016, atmospheric warming and reduced vertical mixing in the Pacific affected global circulation patterns and indirectly influenced atmospheric composition over the Indian Ocean (IO) via atmospheric teleconnections, which in turn modified wind patterns, SST, and convective activity. Although pCO_{2air} is largely controlled by global scale atmospheric CO_2 concentrations, anomalies during certain years such as 2015, 2016, and 2019 may be enhanced due to regional atmospheric dynamics, including weakened monsoon winds and suppressed oceanic CO_2 uptake linked with warmer SST, reduced solubility, and enhanced stratification. These physical conditions inhibit oceanic carbon absorption and can result in higher pCO_{2air} values over the ocean surface. Conversely, La Nina conditions, characterized by intensified upwelling and cooler SST in some parts of the Indian Ocean, may support oceanic CO_2 uptake, slightly moderating the atmospheric CO_2 signal in those years. The relatively uniform spatial distribution across the basin indicates that the atmospheric signal dominates over localized oceanic variations, although coastal and upwelling zones occasionally show minor deviations. The Fig. 5 reveals a latitudinal gradient, with slightly elevated pCO_{2air} levels observed over the

northern AS and BoB in recent years likely due to urban industrial proximity and associated emissions. This consistent year on year rise in pCO_{2air} emphasizes the dominant role of anthropogenic forcing over natural variability in determining atmospheric CO_2 concentrations in the region. Furthermore, the growing atmospheric CO_2 burden has significant implications for air sea CO_2 exchange processes, potentially reducing the ocean capacity to act as a carbon sink in the long term, particularly under warming scenarios. Understanding this interannual variability is crucial for interpreting trends in oceanic carbon fluxes, evaluating feedback mechanisms under climate change, and improving projections of carbon climate interactions in the NIO.

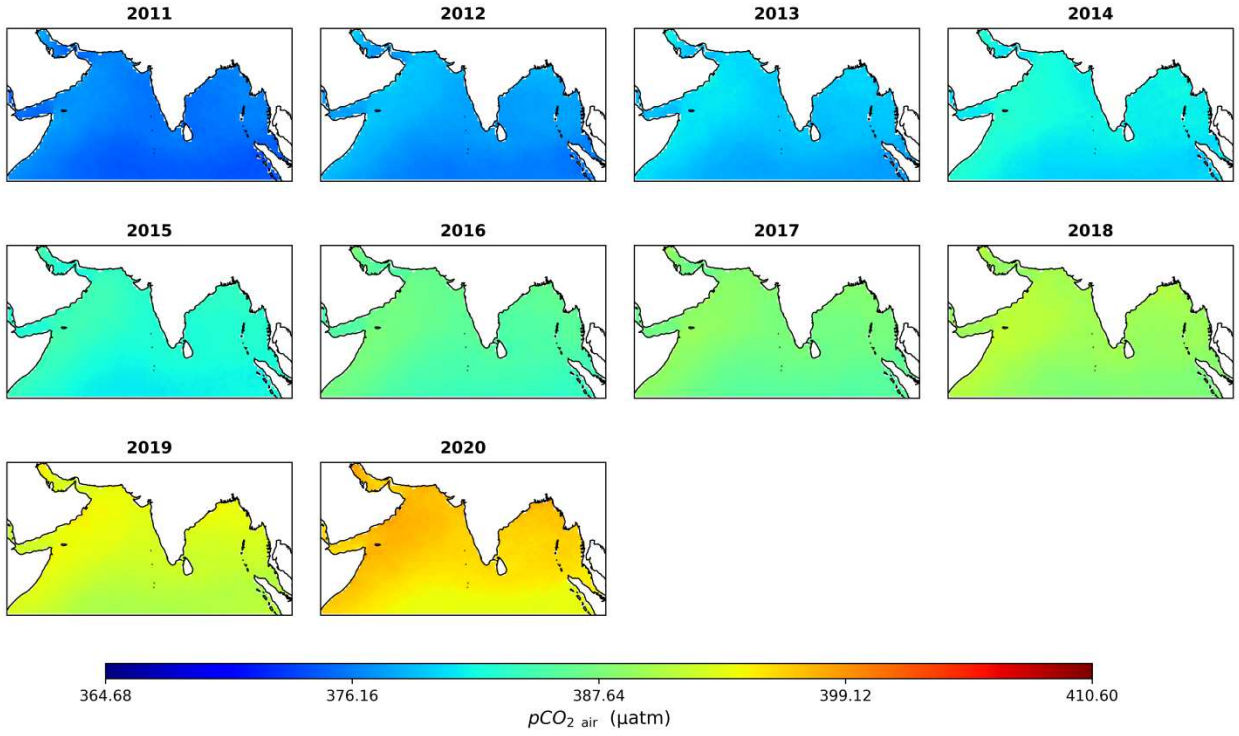


Fig. 5 Interannual variability of pCO_{2air} in the NIO region (2011-2020).

4.2.2. Climatological variability of atmospheric pCO_2 in the NIO region

The climatological distribution of pCO_{2air} over the NIO displays (Fig. 6) a distinct seasonal cycle, closely influenced by atmospheric circulation patterns, regional climatology, and the monsoonal system. Monthly composite maps derived from long term observational datasets reveal clear spatial and temporal variations in pCO_{2air} over the region (Fig. 6). From January through March, the pCO_{2air} values are relatively high across most parts of the NIO. This period corresponds to the northeast monsoon season, characterized by cooler and drier continental air masses blowing seaward. The AS and BoB both exhibit pCO_{2air} values exceeding 387 µatm in

several regions, with localized hotspots in the northern AS, approaching and occasionally exceeding 394 µatm, as indicated by the orange to reddish tones in the maps. These elevated levels are likely a result of continental influence, low precipitation, and reduced convective mixing during this season. With the transition into April and May, pCO_{2air} begins to decline slightly across the basin. The onset of warming and increasing solar radiation contributes to gradual changes in air-sea exchange and the pCO_{2air} values range between 380 and 387 µatm over much of the region. By June, the southwest monsoon becomes dominant, bringing in strong southwesterly winds, increased cloud cover, and heavy rainfall, particularly over the western and eastern coastal margins. During the peak monsoon months of June to August, a clear decline in pCO_{2air} is observed, particularly over the AS and western BoB, where values drop below 380 µatm in many locations, denoted by prominent blue regions in the maps. The influx of moist, marine air masses, coupled with intense convective activity and vertical mixing, contributes to this drawdown in pCO_{2air}. Additionally, the dilution effect due to high precipitation and enhanced biological activity may further lower pCO_{2air} levels near the coastlines. From September through October, the transition from the southwest to northeast monsoon phase is accompanied by a gradual increase in pCO_{2air} .Although the values remain relatively low compared to early winter months, the AS and BoB begin showing signs of pCO_{2air} recovery, particularly in the northern and western sectors. The spatial gradients observed during this time may reflect residual monsoonal effects and lagged responses in air-sea exchange dynamics. By November and December, pCO_{2air} begins to peak again across the NIO, with widespread values between 387 and 394 µatm. This late year increase correlates with the reestablishment of the northeast monsoon, decreased cloud cover, and lower SST, which likely reduce oceanic CO_2 uptake and contribute to higher atmospheric concentrations.

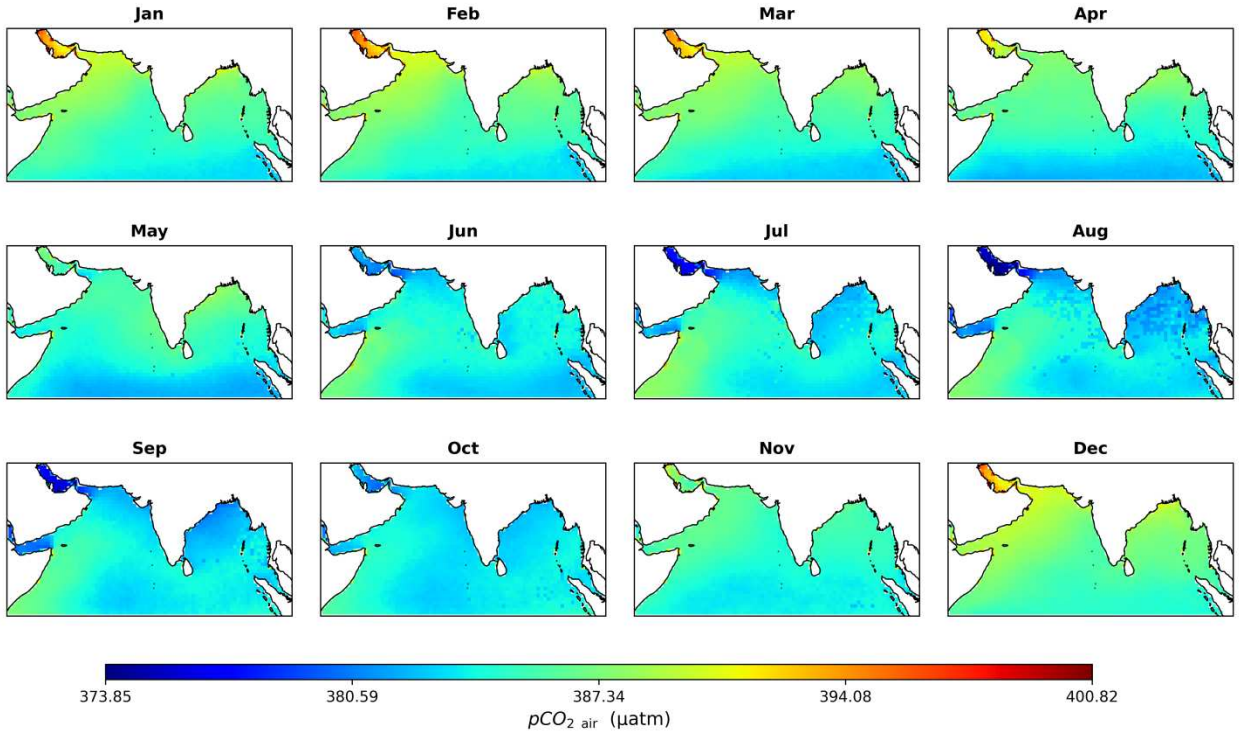


Fig. 6 Climatological variability of pCO_{2air} in the NIO region (2011-2020).

4.3. Interannual variability of air-sea CO_2 flux

The interannual variability of air-sea CO_2 flux across the NIO from 2011 to 2020 (Fig. 7-8) demonstrates pronounced regional and temporal heterogeneity, modulated by both atmospheric and oceanic processes. Fig. 7 presents annual mean spatial distributions of air-sea CO_2 flux, while Fig. 8 provides monthly variability trends across four sub regions: the Andaman Sea, AS, BoB, and Lakshadweep Sea, along with the overall NIO. Fig. 7 indicates a transition in the CO_2 flux regime over the decade, with notable spatial and temporal anomalies. In earlier years such as 2011-2014, the NIO predominantly acted as a net CO_2 source to the atmosphere, as indicated by widespread reddish hues, especially in the western and northern sectors. From 2015 onwards, increased blue shading in the eastern AS and BoB regions suggests a shift towards enhanced oceanic CO_2 uptake in some years, with 2016 and 2020 showing relatively higher sink intensities. These patterns reflect interannual differences in pCO_{2sw} and wind induced gas transfer velocities, likely driven by climatic variability such as ENSO events and IOD phases. Fig. 8 further shows this variability across regional scales. In the Andaman Sea, the air-sea CO_2 flux exhibits a consistent sink like behavior throughout the year, particularly from May to October. This pattern can be attributed to elevated primary productivity and freshwater input

from monsoonal precipitation and riverine discharge, which reduce $pCO2_{sw}$ levels. The variability across years remains relatively constrained, suggesting limited interannual fluctuations in biogeochemical cycling in this semi enclosed basin. The AS, in contrast, displays a complex pattern with both source and sink phases throughout the year. Interannual variability is particularly evident in the months of March-May and October, where some years such as 2015 and 2018 show pronounced emission events. These fluctuations are likely linked to variations in winter convective mixing and pre monsoon upwelling, which bring CO_2 rich subsurface waters to the surface. The anomalous peak in CO_2 flux in 2015 may also be tied to a strong El Nino event, which altered regional wind patterns and surface temperatures.

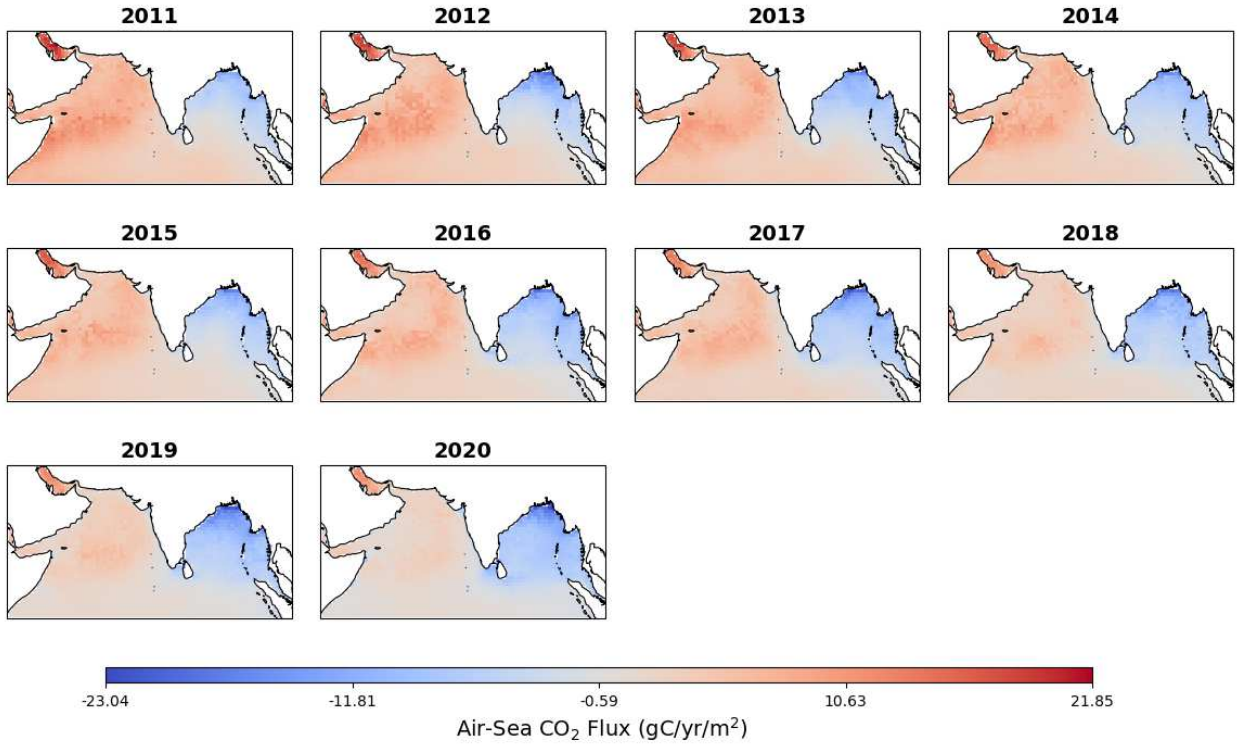


Fig. 7 Interannual variability of air-sea CO_2 flux in the NIO region (2010-2020).

The BoB generally acts as a CO_2 sink, with enhanced uptake during the monsoon and post monsoon periods (June-October). However, interannual variability here is influenced by freshwater stratification, which controls surface water CO_2 concentrations and air-sea exchange efficiency. Notably, 2016 and 2020 display deeper sink intensities, potentially linked to stronger monsoon forcing and stratification-induced suppression of CO_2 rich subsurface mixing. In the Lakshadweep Sea, air-sea CO_2 fluxes remain relatively stable, with minor fluctuations around neutral to weak sink conditions. This region exhibits the least interannual variability among the

sub basins, likely due to its open ocean setting and minimal terrestrial influence. The overall NIO trend in Fig. 8 suggests modest interannual variability, with flux values clustering around a slight net source or near equilibrium. However, specific years such as 2016 and 2020 indicate a basin wide shift towards greater CO_2 uptake, emphasizing the influence of basin scale oceanographic and atmospheric anomalies on carbon flux dynamics.

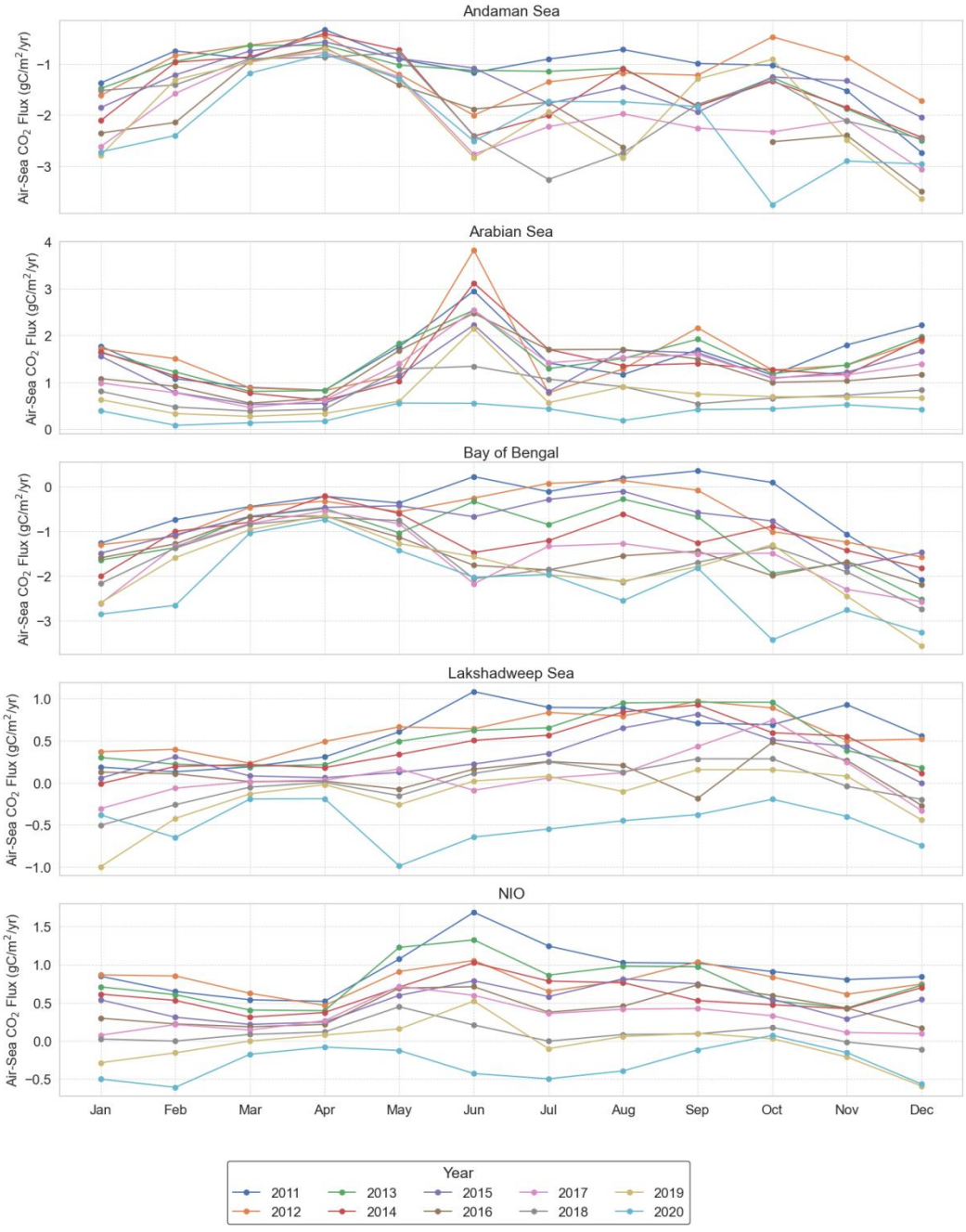


Fig. 8 Climatological variability of air-sea CO_2 flux in sub regions of the NIO (2011–2020).

4.4. Climatological variability of air-sea CO_2 flux

The climatological variability of air-sea CO_2 flux in the NIO, derived from multi-year mean datasets (Fig. 9), demonstrates distinct seasonal and spatial patterns modulated by monsoonal dynamics, regional circulation, and biogeochemical processes. Fig. 9 illustrates the monthly mean spatial distributions of air-sea CO_2 flux, and Fig. 8 shows the monthly climatological trends in the Andaman Sea, AS, BoB, Lakshadweep Sea, and the NIO as a whole. Fig. 9 shows a general seasonal transition in the NIO between net atmospheric CO_2 uptake (blue regions) and source conditions (red regions). During the winter and pre monsoon months (January- May), the basin predominantly acts as a weak to moderate CO_2 sink, particularly evident in the BoB, southeastern AS, and Andaman Sea. These regions exhibit cooler surface waters and enhanced vertical mixing that lower surface pCO_2 levels, favoring oceanic uptake. In contrast, the northern AS and coastal zones show localized emitting during this period, likely driven by convective mixing of CO_2 rich subsurface waters and higher SST. From June through September, during the southwest monsoon, CO_2 flux patterns shift notably. The AS becomes a significant source of CO_2 to the atmosphere, with maximum fluxes observed in June and July (up to ~46.8 $gC/m^2/yr$). This enhancement results from monsoon driven upwelling along the western boundary, which brings subsurface, carbon rich waters to the surface, elevating pCO_2. Additionally, elevated WS during this season increase gas exchange rates, reinforcing the emission. Meanwhile, the BoB and Andaman Sea continue to act as CO_2 sinks, supported by intense freshwater inputs from monsoonal rains and river discharge, which lower surface salinity and suppress pCO_2. By October through December, air-sea CO_2 fluxes begin transitioning back to sink conditions across most of the NIO. The AS gradually weakens as a source, while the BoB and Andaman Sea maintain sink behavior. This seasonal modulation aligns with weakening monsoonal winds, reduced upwelling, and cooling SST, which promote enhanced CO_2 solubility. Fig. 8 complements this spatial assessment by illustrating monthly climatological flux trends across defined regions. In the Andaman Sea, consistent negative fluxes (sink) are observed year round, peaking in June-October, likely due to strong freshwater input and persistent stratification. The **AS** shows strong seasonality, acting as a significant source from May to August, with a pronounced peak in June-July, attributed to upwelling and high wind speeds. The BoB remains a net sink throughout the year, with increased uptake during monsoon and post monsoon months, driven by freshwater stratification and biological productivity. The Lakshadweep Sea exhibits

minimal variability, reflecting its open-ocean nature and reduced biophysical forcing. The aggregated NIO signal shows a net sink phase from September to February, transitioning to a weak source during peak monsoon (June-August), consistent with regional dynamics.

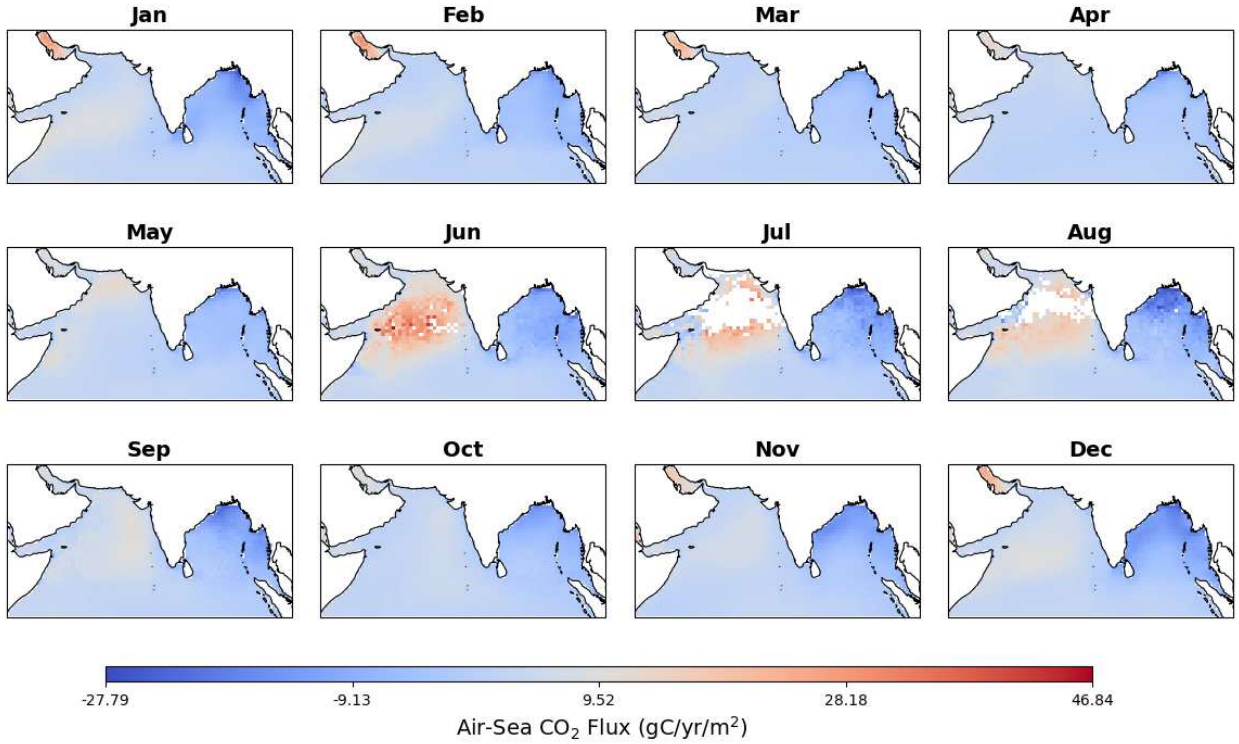


Fig. 9 Climatological variability of air-sea CO_2 Flux in the NIO region (2011–2020).

4.5. Interrelationships among oceanographic variables regulating air-sea CO_2 flux

Fig. 10 demonstrates a scatterplot matrix with Pearson correlation coefficients (r) between five key oceanographic variables: SST, SSS, Chla, ΔpCO_2 and air-sea CO_2 flux. This graphical representation highlights the linear relationships and distributions among these variables, offering insights into the processes governing air-sea CO_2 exchange in the NIO. The strongest positive correlation (r = 0.83) is observed between SST and ΔpCO_2, indicating that warmer sea surface temperatures are associated with a higher ΔpCO_2. This is consistent with established thermodynamic principles, where increasing SST reduces the solubility of CO_2 in seawater, leading to elevated surface pCO_{2sw}. As ΔpCO_2 is a key driver of air-sea CO_2 flux, this positive relationship suggests that warmer waters tend to act as sources of CO_2 to the atmosphere. However, the direct relationship between SST and CO_2 flux is weaker (r = -0.12), possibly due to modulation by other variables such as wind speed, biological activity, and vertical mixing. Chla exhibits strong negative correlations with both ΔpCO_2 (r = -0.80) and SST (r = -0.63). These

results highlight the role of biological processes in CO_2 dynamics. Higher Chla values, indicative of phytoplankton blooms and enhanced primary production, are associated with lower ΔpCO_2. This reflects the biological drawdown of CO_2 during photosynthesis, which reduces pCO_{2sw} in surface waters. The inverse relationship with SST suggests that productive regions in the NIO tend to occur in relatively cooler waters, possibly due to upwelling zones or post monsoon nutrient enrichment events.

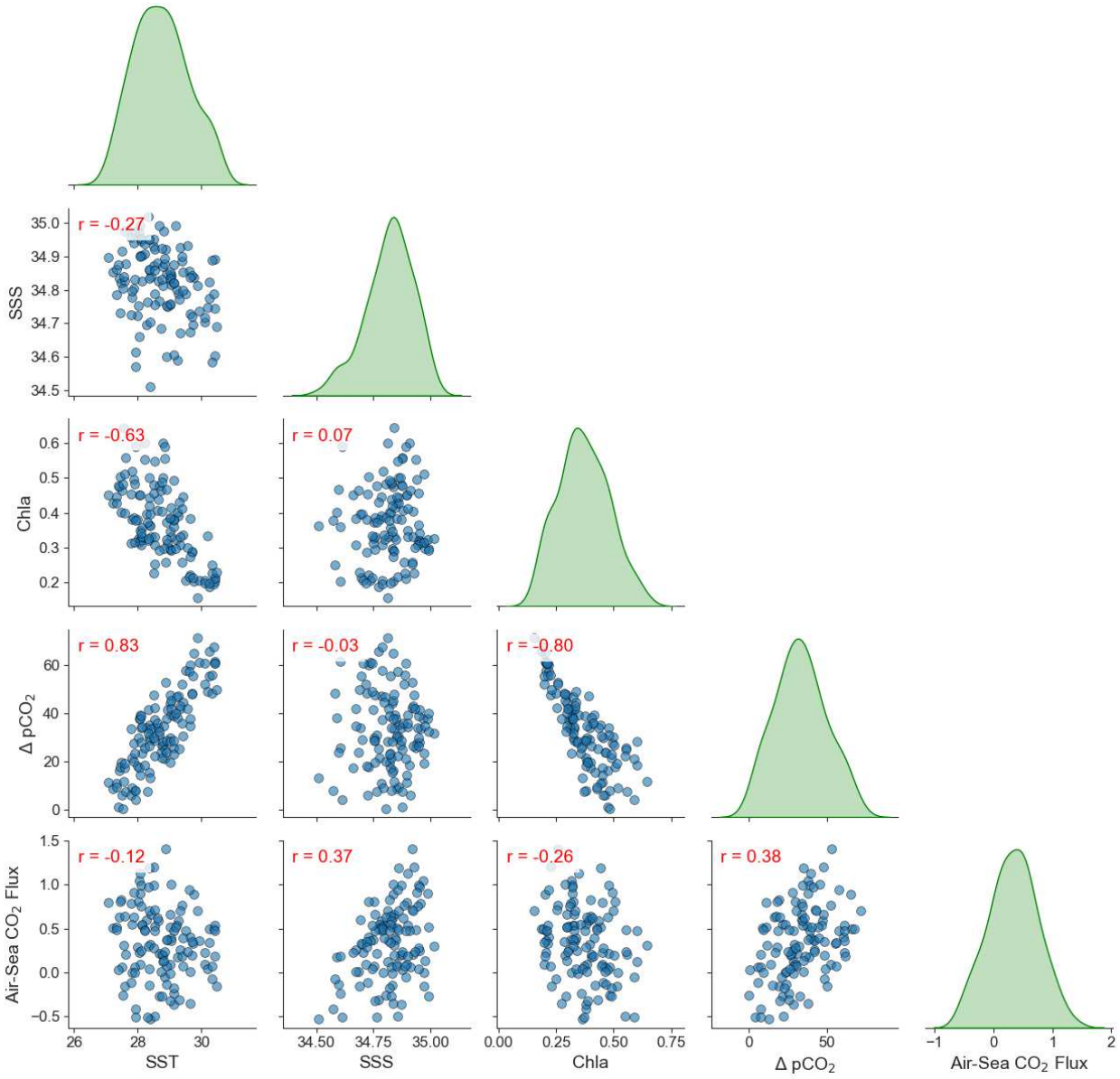


Fig. 10 The scatterplot shows the relationships among oceanographic variables influencing air-sea CO_2 flux.

The relationship between SSS and other variables is comparatively weaker. SSS shows a modest negative correlation with Chla (r = -0.27), which may be linked to freshwater influx from river

discharge or precipitation in productive zones like the BoB. A weak positive correlation with CO_2 flux (r = 0.37) may reflect upwelling induced increases in salinity and CO_2 emission. ΔpCO_2 shows a moderate positive correlation with air-sea CO_2 flux (r = 0.38), reinforcing its role as a direct driver of flux direction and magnitude. Yet, this correlation is not particularly strong, suggesting that ΔpCO_2 alone does not fully determine flux variability. This may be attributed to the influence of gas transfer velocity, wind speed, and other physical drivers not captured in this analysis. The weak negative correlation between Chla and air-sea CO_2 flux (r = -0.26) suggests that biological processes do contribute to the ocean CO_2 uptake capacity, though their net impact may be diluted by physical processes across spatial and temporal scales. Fig. 10 emphasize the complexity of air-sea CO_2 exchange in the NIO, with SST and biological productivity (Chla) emerging as dominant influencers. The results highlight the importance of accounting for both physical and biological processes in carbon cycle studies, particularly in monsoon affected tropical marine systems where these drivers interact dynamically.

4.6. Comparative assessment of air-sea CO_2 flux estimates in the NIO

The estimated air-sea CO_2 flux from this study over the NIO is approximately 0.06 ± 0.02 Pg C yr^{-1}, indicating a net CO_2 source to the atmosphere. This value is compared here with previous observational and model-based estimates across similar regions to provide context and assess consistency. Bates (2006) estimated the annual CO_2 flux for the entire Indian Ocean at 0.24 ± 0.13 Pg C yr^{-1}, suggesting a stronger source of CO_2. When narrowed down to sub basins, Bates reported 0.064 ± 0.01 Pg C yr^{-1} for the AS and 0.013 ± 0.005 Pg C yr^{-1} for the BoB, which align reasonably well with this study regional scale. Sarma et al. (2023), in a more recent assessment, estimated CO_2 fluxes north of 18°S at 0.04 ± 0.05 Pg C yr^{-1}, and south of 18°S at −0.23 ± 0.11 Pg C yr^{-1}, indicating that the southern Indian Ocean acts as a CO_2 sink, while the northern portion remains a weak source. These regional disparities are largely driven by variations in ocean circulation, biological activity, and monsoonal dynamics that influence CO_2 solubility and gas exchange. The findings from this study fall within the range of previous estimates, particularly aligning with those of Sarma et al. (2023) for the northern sector. The close agreement reinforces the robustness of the observational approach used here. However, the estimate from this study is slightly higher than Sarma et al. (2023) northern component, possibly due to differences in temporal coverage, resolution, and data assimilation techniques. The Fig. 11 demonstrates these comparisons, highlighting not only the differences in absolute values but also

the uncertainty margins associated with each estimate. This comparative analysis is useful for improving model validation and understanding the regional role of the Indian Ocean in the global carbon cycle.

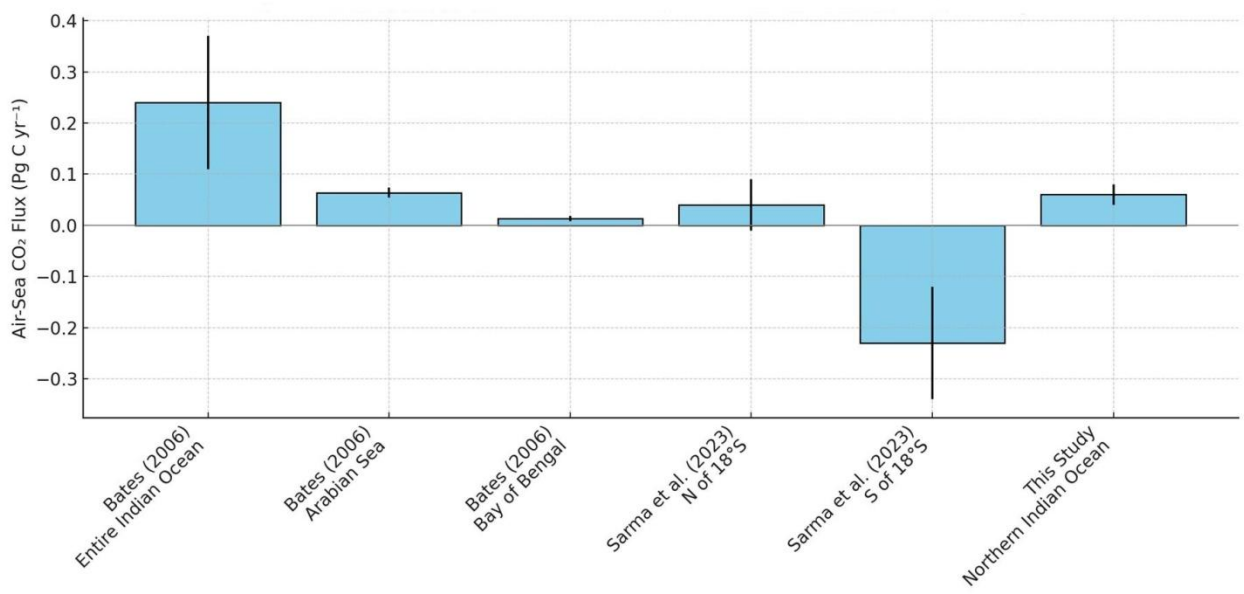


Fig. 11 Comparison of air-sea CO_2 flux estimates in the Indian Ocean region.

4.7. Limitations and scope of the future work

The present analysis relies on only five variables (SST, SSS, Chla, WS, and SLP); however, pCO_{2sw} is also significantly influenced by total alkalinity (TA), dissolved inorganic carbon (DIC), and ocean circulation. Incorporating these additional variables can enhance model performance and reduce uncertainties in the results. Furthermore, the use of advanced analytical methods, such as deep learning (DL), can further improve the accuracy and robustness of the estimations (Ghoshal et al., 2025). According to Sarma et al. (2013), upwelling plays a major role in determining pCO_{2sw} levels, particularly along the western boundaries of oceanic basins, where nutrient rich deep waters rise to the surface due to the Coriolis effect. This process elevates surface DIC and, consequently, pCO_{2sw} concentrations. Therefore, accounting for DIC and TA is essential for more realistic pCO_{2sw} estimations. Additionally, the number of available in-situ observations for regression modeling is relatively low in the NIO compared to other ocean basins like the Atlantic and Pacific. This sparse data coverage limits the accuracy and representativeness of existing models. Hence, there is an imperative need for more frequent and

spatially comprehensive pCO_{2sw} measurements across the NIO, especially given the regions complex and heterogeneous biogeochemical conditions.

5. Conclusion

This study aims to explore the air-sea CO_2 exchange in the NIO region by utilizing satellite-derived datasets and models to estimate surface pCO_{2sw} and compute CO_2 fluxes across marginal seas such as the AS, Andaman Sea, BoB, and Lakshadweep Sea, as well as adjoining regions like the Persian Gulf, Equatorial Indian Ocean, and Gulf of Oman. The analysis reveals significant spatial variability in carbon cycling patterns across the region. The study investigates how various oceanographic and atmospheric variables such as SST, SSS, Chla, WS, atmospheric CO_2, and SLP influence pCO_{2sw} variability and air-sea CO_2 fluxes. It was found that the AS and Persian Gulf generally act as CO_2 sources to the atmosphere, while the BoB and Andaman Sea tend to function as CO_2 sinks. The Lakshadweep Sea exhibits dual behavior, acting as both a source and sink depending on seasonal and spatial conditions, likely due to its intermediate position between these basins. These regional characteristics are influenced by a combination of freshwater input, salinity gradients, biological activity, and surface water temperature. The study also highlights an inverse relationship between air-sea CO_2 flux and atmospheric CO_2 concentration, indicating a shift toward saturation between oceanic and atmospheric CO_2 levels. SST and Chla are identified as primary drivers of pCO_{2sw} variability, while salinity plays a more indirect role by affecting both the direction and magnitude of the flux. Satellite observations provide spatially continuous and high-resolution data that help overcome the limitations of sparse and unevenly distributed in-situ measurements in the NIO region. However, the study acknowledges uncertainties due to the exclusion of key carbon system drivers such as TA and DIC ocean currents, and upwelling processes. To enhance model accuracy, the incorporation of these additional variables is recommended. Developing robust models that are less dependent on in-situ datasets will also help reduce uncertainties. The findings of this study provide valuable insights that can inform future projections and support the development of climate policies aimed at mitigating anthropogenic impacts on oceanic carbon uptake. Future research should focus on expanding the set of influencing variables, refining predictive models, and enhancing monitoring systems to support sustainable marine ecosystem management and long term carbon regulation strategies.

Acknowledgement

The authors would like to express their sincere gratitude to the Director of the National Remote Sensing Centre (NRSC) for providing the opportunity to carry out this project at the Earth and Climate Sciences Area (ECSA). We also acknowledge the use of satellite derived datasets from NASA Ocean Color Web and the Copernicus Marine Environment Monitoring Service (CMEMS).

Data availability statement

The study was carried out using freely available datasets and the sources are mentioned below. The analysis and maps are generated using Jupyter Lab (Python).

(Sea Surface Salinity: https://doi.org/10.48670/moi-00021; Sea Surface Temperture: https://oceancolor.gsfc.nasa.gov/l3/; Chlorophyll concentration: https://oceancolor.gsfc.nasa.gov/l3/;Wind Speed: https://doi.org/10.48670/moi-00181; Atmospheric CO_2: https://ads.atmosphere.copernicus.eu/datasets/cams-global-ghg-reanalysis-egg4; Sea level Pressure: https://ads.atmosphere.copernicus.eu/datasets/cams-global-ghg-reanalysis-egg4).

Declaration of interest statement

The authors declare that there is no conflict of interest.

Author contribution statement

Nandha Kumar M.: Data curation, Visualization, and Methodology; Mukeem Thoufiq Ahmed: Data Analysis and Validation; Nazeera Begum Pathan: Validation, Data curation and Conceptualization; P. Brahmaji Rao: Supervision; Ibrahim Shaik: Data curation, Original manuscript writing, and Validation; Mahesh Pathakoti: Supervision and manuscript editing.

Funding statement

There is no funding involved in the study.

References

Antony, S., Dev, V. V., Kumar, M. R., & Krishnan, K. A. (2021). Composition and distribution pattern of plankton communities in lagoon and offshore region of Kavaratti Atoll, Lakshadweep Archipelago, India. *Sustainable Water Resources Management*, *7*(6), 93.

Bakker, D. C., Pfeil, B., Landa, C. S., Metzl, N., O'brien, K. M., Olsen, A., ... & Xu, S. (2016). A multi-decade record of high-quality fCO 2 data in version 3 of the Surface Ocean CO 2 Atlas (SOCAT). *Earth System Science Data*, *8*(2), 383-413.

Bates, N. R., Pequignet, A. C., & Sabine, C. L. (2006). Ocean carbon cycling in the Indian Ocean: 1. Spatiotemporal variability of inorganic carbon and air-sea CO2 gas exchange. *Global Biogeochemical Cycles*, *20*(3).

Bates, N. R., Moran, S. B., Hansell, D. A., & Mathis, J. T. (2006). An increasing CO2 sink in the Arctic Ocean due to sea-ice loss. *Geophysical Research Letters*, *33*(23).

Boyd, P. W., Claustre, H., Levy, M., Siegel, D. A., & Weber, T. (2019). Multi-faceted particle pumps drive carbon sequestration in the ocean. *Nature*, *568*(7752), 327-335.

Ciais, P., Sabine, C., Bala, G., Bopp, L., Brovkin, V., & House, J. I. (2014). Carbon and other biogeochemical cycles. In *Climate Change 2013: The Physical Science Basis. Contribution of Working Group I to the Fifth Assessment Report of the Intergovernmental Panel on Climate Change Change* (pp. 465-570). Cambridge University Press.

DeVries, T., Le Quéré, C., Andrews, O., Berthet, S., Hauck, J., Ilyina, T., ... & Séférian, R. (2019). Decadal trends in the ocean carbon sink. *Proceedings of the National Academy of Sciences*, *116*(24), 11646-11651.

Doney, S. C., Busch, D. S., Cooley, S. R., & Kroeker, K. J. (2020). The impacts of ocean acidification on marine ecosystems and reliant human communities. *Annual Review of Environment and Resources*, *45*(1), 83-112.

Flanders Marine Institute (2018). IHO Sea Areas, version 3. Available online at https://www.marineregions.org/.

Flanders Marine Institute. (2019). Maritime boundaries geodatabase: Maritime boundaries and exclusive economic zones (200NM), version 11.

Friedlingstein, P., O'sullivan, M., Jones, M. W., Andrew, R. M., Hauck, J., Landschützer, P., ... & Zeng, J. (2024). Global carbon budget 2024. *Earth System Science Data Discussions*, *2024*, 1-133.

Gauns, M., Madhupratap, M., Ramaiah, N., Jyothibabu, R., Fernandes, V., Paul, J. T., & Kumar, S. P. (2005). Comparative accounts of biological productivity characteristics and estimates of carbon fluxes in the Arabian Sea and the Bay of Bengal. *Deep Sea Research Part II: Topical Studies in Oceanography*, *52*(14-15), 2003-2017.

Ghoshal, P. K., Joshi, A. P., & Chakraborty, K. (2025). An improved long-term high-resolution surface p CO2 data product for the Indian Ocean using machine learning. *Scientific Data*, *12*(1), 577.

Gruber, N., Clement, D., Carter, B. R., Feely, R. A., Van Heuven, S., Hoppema, M., ... & Wanninkhof, R. (2019). The oceanic sink for anthropogenic CO2 from 1994 to 2007. *Science*, *363*(6432), 1193-1199.

Joshi, A. P., Ghoshal, P. K., Chakraborty, K., & Sarma, V. V. S. S. (2024). Sea-surface p CO2 maps for the Bay of Bengal based on advanced machine learning algorithms. *Scientific Data*, *11*(1), 384.

Khatiwala, S., Tanhua, T., Mikaloff Fletcher, S., Gerber, M., Doney, S. C., Graven, H. D., ... & Sabine, C. L. (2013). Global ocean storage of anthropogenic carbon. *Biogeosciences*, *10*(4), 2169-2191.

Krishna, K. V., Shanmugam, P., & Nagamani, P. V. (2020). A multiparametric nonlinear regression approach for the estimation of global surface ocean pCO 2 using satellite oceanographic data. *IEEE Journal of Selected Topics in Applied Earth Observations and Remote Sensing*, *13*, 6220-6235.

Kumar, S., Ramesh, R., Sardesai, S., & Sheshshayee, M. S. (2004). High new production in the Bay of Bengal: Possible causes and implications. *Geophysical Research Letters*, *31*(18).

Landschützer, P., Gruber, N., Haumann, F. A., Rödenbeck, C., Bakker, D. C., Van Heuven, S., ... & Wanninkhof, R. (2015). The reinvigoration of the Southern Ocean carbon sink. *Science*, *349*(6253), 1221-1224.

Le Quéré, C., Andrew, R. M., Friedlingstein, P., Sitch, S., Hauck, J., Pongratz, J., ... & Zheng, B. (2018). Global carbon budget 2018. *Earth System Science Data*, *10*(4), 2141-2194.

Madhupratap, M., Kumar, S. P., Bhattathiri, P. M. A., Kumar, M. D., Raghukumar, S., Nair, K. K. C., & Ramaiah, N. (1996). Mechanism of the biological response to winter cooling in the northeastern Arabian Sea. *Nature*, *384*(6609), 549-552.

Naqvi, S. W. A., Moffett, J. W., Gauns, M. U., Narvekar, P. V., Pratihary, A. K., Naik, H., ... & Ahmed, S. I. (2010). The Arabian Sea as a high-nutrient, low-chlorophyll region during the late Southwest Monsoon. *Biogeosciences*, *7*(7), 2091-2100.

Nightingale, P. D., Malin, G., Law, C. S., Watson, A. J., Liss, P. S., Liddicoat, M. I., ... & Upstill-Goddard, R. C. (2000). In situ evaluation of air-sea gas exchange parameterizations using novel conservative and volatile tracers. *Global Biogeochemical Cycles*, *14*(1), 373-387.

Ocean to monsoonal forcing. *Deep-sea research. Part II, Topical studies in oceanography*, *45*(10-11), 1905-1915.

Pérez, F. F., et al. (2013). Atlantic Ocean CO_2 uptake reduced by weakening of the meridional overturning circulation. *Nature Geoscience*, *6*(2), 146–152.

Prasanna Kumar, S., Divya David, T., Byju, P., Narvekar, J., Yoneyama, K., Nakatani, N., ... & Mizuno, K. (2012). Bio-physical coupling and ocean dynamics in the central equatorial Indian Ocean during 2006 Indian Ocean Dipole. *Geophysical research letters*, *39*(14).

Resplandy, L., Séférian, R., & Bopp, L. (2015). Natural variability of CO2 and O2 fluxes: What can we learn from centuries-long climate models simulations?. *Journal of Geophysical Research: Oceans*, *120*(1), 384-404.

Rixen, T., Cowie, G., Gaye, B., Goes, J., do Rosário Gomes, H., Hood, R. R., ... & Singh, A. (2020). Reviews and syntheses: Present, past, and future of the oxygen minimum zone in the northern Indian

Ocean. Biogeosciences, 17(23), 6051-6080. Sabine, C. L., et al. (2004). The oceanic sink for anthropogenic CO_2. *Science*, *305*(5682), 367–371.

Sabine, C. L., Feely, R. A., Gruber, N., Key, R. M., Lee, K., Bullister, J. L., ... & Rios, A. F. (2004). The oceanic sink for anthropogenic CO2. *science*, *305*(5682), 367-371.

Sarma, V. V. S. S., Sridevi, B., Nair, T. B., Lotliker, A. A., Baliarsingh, S. K., & Rao, E. P. R. (2025). Tropical cyclones enhance net CO2 sink in the Bay of Bengal. *Progress in Oceanography*, *231*, 103422.

Sarma, V. V. S. S., Sridevi, B., Metzl, N., Patra, P. K., Lachkar, Z., Chakraborty, K., ... & Chandra, N. (2023). Air-Sea fluxes of CO2 in the Indian Ocean between 1985 and 2018: A synthesis based on Observation-based surface CO2, hindcast and atmospheric inversion models. *Global Biogeochemical Cycles*, *37*(5), e2023GB007694.

Sarma, V. V. S. S., Kumar, M. D., & George, M. D. (1998). The central and eastern Arabian Sea as a perennial source of atmospheric carbon dioxide. *Tellus B: Chemical and Physical Meteorology*, *50*(2), 179-184.

Sarma, V. V. S. S., Lenton, A., Law, R. M., Metzl, N., Patra, P. K., Doney, S., ... & Valsala, V. (2013). Sea–air CO2 fluxes in the Indian Ocean between 1990 and 2009. *Biogeosciences*, *10*(11), 7035-7052.

Schott, F. A., & McCreary Jr, J. P. (2001). The monsoon circulation of the Indian Ocean. *Progress in Oceanography*, *51*(1), 1-123.

Smith, S. L., Codispoti, L. A., Morrison, J. M., & Barber, R. T. (1998). The 1994-1996 Arabian Sea Expedition: An integrated, interdisciplinary investigation of the response of the northwestern Indian

Sutton, A. J., Feely, R. A., Maenner-Jones, S., Musielwicz, S., Osborne, J., Dietrich, C., ... & Weller, R. A. (2019). Autonomous seawater pCO 2 and pH time series from 40 surface buoys and the emergence of anthropogenic trends. *Earth System Science Data*, *11*(1), 421-439.

Shaik, I., Krishna, K. V., Begum, S. K., Suhail, K. M., Nagamani, P. V., Shanmugam, P., ... & Srivathsav, K. (2023). Advancements in Carbon Dioxide Modeling: An Algorithm Incorporating In-Situ and Satellite Data for Improved Understanding of pCO Dynamics in the Bay of Bengal. *IEEE Access*, *11*, 144877-144886.

Shaik, I., Fathima, M. F., Nagamani, P. V., Yadav, S., Behera, S., Manmode, Y., & Rao, G. S. (2025). Satellite-Derived Ocean Color Data for Monitoring pCO2 Dynamics in the North Indian Ocean. *Dynamics of Atmospheres and Oceans*, 101534.

Takahashi, T., Sutherland, S. C., Wanninkhof, R., Sweeney, C., Feely, R. A., Chipman, D. W., ... & de Baar, H. J. (2009). Climatological mean and decadal change in surface ocean pCO2, and net sea–air CO2 flux over the global oceans. *Deep Sea Research Part II: Topical Studies in Oceanography*, *56*(8-10), 554-577.

Valsala, V., & Murtugudde, R. (2015). Mesoscale and intraseasonal air–sea CO2 exchanges in the western Arabian Sea during boreal summer. *Deep Sea Research Part I: Oceanographic Research Papers*, *103*, 101-113.

Wanninkhof, R. (1992). Relationship between wind speed and gas exchange over the ocean. *Journal of Geophysical Research: Oceans*, *97*(C5), 7373-7382.

Wanninkhof, R., Park, G. H., Takahashi, T., Sweeney, C., Feely, R., Nojiri, Y., ... & Khatiwala, S. (2013). Global ocean carbon uptake: magnitude, variability and trends. *Biogeosciences*, *10*(3), 1983-2000.

Wanninkhof, R. (2014). Relationship between wind speed and gas exchange over the ocean revisited. *Limnology and Oceanography: Methods*, *12*(6), 351-362.

Yang, S., Li, Z., Yu, J. Y., Hu, X., Dong, W., & He, S. (2018). El Niño–Southern Oscillation and its impact in the changing climate. *National Science Review*, *5*(6), 840-857.